Check for updates

β-Lactoglobulin–chlorogenic acid conjugate-based nanoparticles for delivery of (−)-epigallocatechin-3-gallate

Yuting Fan,[a] Yuzhu Zhang,[b] Wallace Yokoyama[b] and Jiang Yi (ID) *[a]

β-Lactoglobulin (BLG)–chlorogenic acid (CA) conjugates were generated by a free radical induced grafting method. BLG–CA conjugates showed better antioxidant activities than BLG. The antioxidant activity increased with the increase of CA substitution. The particle sizes of (−)-epigallocatechin-3-gallate (EGCG)-loaded nanoparticles prepared by the anti-solvent method were 110.3, 107.4, and 105.8 nm for BLG, BLG–CA (low), and BLG–CA (high), respectively. The encapsulation efficiencies of EGCG in BLG, BLG–CA conjugate (low), and BLG–CA conjugate (high) nanoparticles were 72.9%, 71.8%, and 73.5%, respectively. The chemical stabilities of EGCG in both BLG–CA nanoparticles were significantly higher than in BLG nanoparticles. BLG–CA conjugate (high) showed better EGCG retention than BLG–CA conjugate (low) in simulated gastrointestinal digestion fluid. Little EGCG was released in both BLG nanoparticles and BLG–CA nanoparticles under simulated gastric digestion. The release of EGCG in BLG–CA nanoparticles was less than that in BLG nanoparticles, indicating that CA conjugating protected BLG from the digestive enzymes.

Introduction

(−)-Epigallocatechin-3-gallate (EGCG) is the most active catechin of tea polyphenols. It accounts for 50–80% of the total catechin present in green tea.[1,2] Potential health-promoting properties of EGCG include strong antioxidant activity, cancer chemoprevention, radioprotection, cardiovascular health improvement, anti-obesity ability.[3–5] EGCG was reported to be approximately 10 times as effective as β-carotene, and L-ascorbate in alkyl peroxyl radical scavenging.[6] It was more effective than TBHQ in preventing fish meat from oxidizing ($p < 0.05$).[3] EGCG was also reported to have anticancer effects through suppressing angiogenesis by blocking the induction of vascular endothelial growth factor (VEGF) in human colon carcinoma cells.[7]

However, EGCG's bioactivity is limited by its low oral bioavailability, and poor stability. EGCG is highly soluble in water. It can be easily oxidized in aqueous phase. Thus, it is an unstable bioactive compound, especially under neutral and alkaline conditions. In a phosphate buffer (PB, pH 7.4), more than 80% of EGCG was quickly degraded in only 3 h.[8] The increase of either pH, oxygen concentration or storage temperature accelerated its degradation. The bioabsorption of EGCG was less than 1.1% after oral administration.[9,10] Recent

studies showed that the absorption of EGCG was enhanced when delivered in nanoparticles. The result was mainly attributed to the stabilization of EGCG in nanoparticles rather than the effect of nanoparticles on intestinal transport or on efflux proteins.[9]

EGCG can be protected against chemical degradation or oxidation by nano-encapsulation with proteins mainly through hydrophilic and hydrophobic interactions.[11–13] Even though the chemical stability of EGCG in protein nanoparticles can be significantly improved, more than 30% of EGCG was oxidized during only 10 days of storage at 4 °C in the dark.[13] Predictably, EGCG oxidation will be accelerated when stored at room temperature or higher temperature or exposed to light. Furthermore, the early release during in vitro digestion due to proteolysis also facilitated the oxidation or degradation and resulted in poor bioavailability.

β-Lactoglobulin (BLG), a ligand-binding protein, was extensively studied. BLG is the most abundant whey protein.[14] It was widely used for encapsulating bioactive molecules to enhance their bioavailability.[15,16] Among all tea polyphenols, EGCG exhibited the highest affinity for BLG.[17] Recent studies showed that thermal treatment (75–85 °C) of BLG led to the increase of its affinity for EGCG by 3.5-fold due to the exposure of hydrophobic amino acid residues. Compared with native BLG, encapsulation with thermal treatment BLG resulted in improved of chemical stability of EGCG and better protection of its antioxidant activity.[18–20] This may be mainly due to the increased thiol group, more exposed hydrophobic group of protein, and more EGCG bound to protein after heat

[a]Department of Food Science and Engineering, College of Chemistry and Environmental Engineering, Shenzhen University, Shenzhen, Guangdong, 518060, China. E-mail: yijiangjnu@gmail.com; Fax: +86-755-26536141; Tel: +86-755-26557377

[b]Western Regional Research Center, ARS, USDA, Albany, California 94710, USA

treatment.[21] The functional properties (heat-induced insolubility, emulsifying activity, gelling property, and calcium phosphate solubilizing ability) of BLG can also be remarkably improved with glycation and phosphorylation.[14,22] Our previous study showed that BLG is resistant to pepsin hydrolysis partly due to its compact structure with almost 50% of β-sheet.[23] Whereas it can be digested by trypsin. Pepsin and trypsin are the main proteases in human digestive system. Pepsin, acted in the stomach, is specialized in hydrolyzing peptide bonds between hydrophobic and preferably aromatic amino acids (Phe, Trp, and Tyr). Whereas trypsin, produced in the small intestine, mainly cleaves proteins on the carboxyl side of the amino acids (Lys or Arg).[24,25] Recently, it was reported that protein–polyphenols conjugates with potential antioxidant activity can be obtained through free radical induced grafting method.[26–28]

Nevertheless, the potential of these protein–phenolic conjugates in the development of nanoparticles delivery systems for labile hydrophilic molecules has not been well investigated. Study in our group found that compared to BLG, BLG–catechin conjugate exhibited better protection against β-carotene oxidation in nanoemulsion.[28]

In this study, conjugation between BLG and chlorogenic acid (CA) was optimized with various mass ratio of BLG : CA. The obtained BLG–CA conjugate was characterized with SDS-PAGE, far UV CD, and ATR-FTIR. EGCG-loaded BLG and BLG–CA nanoparticles were prepared with an anti-solvent method and the storage stability was compared. *In vitro* release profile and digestive stability of EGCG was also investigated under simulated gastrointestinal tract. The goal of this paper was to study the potential of BLG–CA conjugates used as nano-delivery matrices for protecting and delivering of bioactive nutraceuticals.

Materials and methods

Bovine beta-lactoglobulin (≥90%, L0130), chlorogenic acid, L-ascorbic acid, hydrogen peroxide (30%, w/w), DPPH, AAPH, fluorescein, and Trolox, were obtained from Sigma-Aldrich (St. Louis, MO). EGCG (purity > 95% by HPLC) was purchased from Chuangsai Co., Ltd. (Shanghai, China). All other analytical grade chemicals and reagents were obtained from Sinopharm Chemical Reagent Co., Ltd. (Shanghai, China).

Preparation of BLG–CA conjugates

BLG–CA conjugates were produced with a free radical method as previously reported[26] with slight modifications. In brief, 0.5 g BLG was fully dissolved in 50 mL distilled water, then, 0.5 mL of 10.0 M H_2O_2 and 0.25 g L-ascorbic acid (1.4 mmol) were added gradually, while the mixture was stirred at 25 °C under atmospheric air. After 2 h, different amount of CA was added to aliquots of the mixture (at the mass ratios of CA to BLG: 0.1 : 1, 0.25 : 1, 0.5 : 1, 0.75 : 1, and 1 : 1, respectively). After 24 h, the free unreacted CA in reaction solution was removed by dialysis against ultrapure water 10 times the volume of the reaction solution. The dialysis bags had a 3 kDa molecular weight cutoffs for proteins. The dialysis was carried out for 48 h at 4 °C with 10

water changes. RP-HPLC results showed that no free CA or free L-ascorbic acid could be detected in the dialyzed conjugate solutions. The remaining BLG–CA conjugates solution was lyophilized (Labconco, MO) and stored in a freezer for further use.

Evaluation of phenolic groups by Folin–Ciocalteu reagent

The CA amount in BLG–CA conjugates was analyzed with previous protocols with minor modification.[29] In brief, 0.5 mL of BLG–CA conjugates was mixed with 1 mL of Folin–Ciocalteu reagent for 5 min in the dark, then 2 mL of 20% sodium carbonate (Na_2CO_3) was added. The mixture was vortexed and incubated 1 h at room temperature. The absorbance was recorded with Nanodrop 2000c (Thermos-Scientific, U.S.) at a wavelength of 747 nm. Gallic acid was used as a standard. The conjugating amounts of BLG–CA conjugates were expressed as milligrams of gallic acid equivalent per gram of conjugates.

Characterization of BLG–CA conjugates

Sodium dodecyl sulfate polyacrylamide gel electrophoresis (SDS-PAGE). SDS-PAGE analysis under reducing condition was performed at a constant voltage of 120 V according to an established protocol.[30] A 4–20% gradient polyacrylamide gel was used for the separation of BLG (control), and BLG–CA conjugates. Samples were heated in an SDS sample buffer (50 mM Tris–HCl, pH 6.8, 2% SDS, 0.1% bromophenol blue, 10% glycerol) containing 100 mM β-mercaptoethanol for 5 min at 95 °C before loading. Loading volume of samples was 20 μL (protein content was 25.0 μg). The Colloidal Coomassie G-250 Staining protocols were used for the gels staining.[31] A Chemilmager™ 4400 (Alpha Innotech, CA, U.S.) was used to scan the stained gel.

Far UV circular dichroism (CD). The secondary structure changes of the protein after conjugation was determined by a J-815 CD spectrometer (Jasco, Tokyo) between 195 and 260 nm based on a method described previously.[32] A cell with a 2.0 mm path length was used. Samples (protein concentration is 0.2 mg mL^{-1}) prepared with 10 mM PB (pH 7.0) were used and the PB solution was used as the blank for all samples. The scan rate was 50 nm min^{-1} at 20 °C. Ten scans were averaged. The results were displayed as mean residue ellipticity (degrees per cm^2 per dmol) using 162 for the average number of amino acid residues per molecule of BLG.[33]

Attenuated total reflectance-Fourier transform infrared spectroscopy (ATR-FTIR). Infrared spectra were obtained at room temperature with ATR-FTIR spectrophotometer (Nicolet iS10, Thermo-Scientific, Madison, WI) in the frequency range of 4000–650 cm^{-1}. All spectra were collected at 4 cm^{-1} resolution. A background spectrum was obtained for each sample. The powder sample was placed at the center of the crystal surface. Two hundreds and fifty-six scans were accumulated.

For analyzing the secondary structure of BLG and BLG–CA conjugate, the IR spectra (1700 to 1600 cm^{-1}) were further subjected to Fourier self-deconvolution (FSD) using the OMNIC software (Thermo Scientific, West Palm Beach, FL, USA). The FSD spectra were then curve fitted assuming a Gaussian band

profile. The FTIR deconvolution spectra were curve-fitted by Gaussian–Lorentzian function with PeakFit software (Version 4.12, SeaSolve Software Inc., Framingham, MA). Peak assignment was carried out on the FSD spectra following literatures on native BLG, and the content of each secondary structure was expressed as the percentage of area of the corresponding peaks.[34]

DPPH radical scavenging activity. The 2,2-diphenyl-1-picrylhydrazil (DPPH) radical scavenging activity of BLG, BLG–CA (low), BLG–CA (high), and CA were determined according to the method reported previously.[30] The absorbance was recorded at 517 nm.

Ferric reducing power. The reducing power of BLG, BLG–CA (low), BLG–CA (high), and CA was measured as described in our previous reports with slight modifications.[30] The absorbance was detected at 700 nm.

Oxygen radicals antioxidant capacity. The antioxidant capacity of BLG, BLG–CA (low), BLG–CA (high), and CA was analyzed with oxygen radicals antioxidant capacity assay, based on a previous method.[35] In each well, 50 µL of fluorescein (70 nM) and 50 µL (5 µg mL^{-1}) of sample, control (PB, pH 7.0), or standard (trolox, 20 µM) were mixed. The mixture was kept at 37 °C for 15 min, and then 25 µL of AAPH (221 mM) were added. The 96-well plate was placed into a fluorescence Multilabel microplate counter (Victor3, PerkinElmer, MA, U.S.). The fluorescence was recorded at 535 nm every 5 min for 90 min at 37 °C with the excitation at 485 nm. The ORAC values of all samples were expressed as µM Trolox equivalents (µM TE).

$$ORAC \ (\mu M \ TE) = \frac{C_t \times (AUC_s - AUC_b) \times k}{(AUC_t - AUC_b)} \quad (1)$$

where C_t is the concentration (µM) of Trolox (20 µM), k is the sample dilution factor, and AUC is the area below the fluorescence decay curve of the sample, blank, and Trolox, respectively.

$$AUC = 1 + \sum_{i=1}^{i=90} \frac{f_{i/5}}{f_0} \quad (2)$$

where f_0 is the initial fluorescence and $f_{i/5}$ is the fluorescence at time $i/5$.

EGCG nanoparticle preparation. BLG-EGCG and BLG–CA-EGCG nanoparticles were prepared by a method that has previously been described with minor modifications.[36] BLG or BLG–CA conjugates (20 mg mL^{-1}) were fully dissolved in ultrapure water, respectively, and the pH was adjusted to 9.0. Pure acetone was added dropwise to BLG or BLG–CA conjugate solution. Final acetone/water ratio was 80 : 20 (v/v). After desolvation, glutaraldehyde was added and sample was incubated with stirring for 2 h. Acetone was removed with an evaporator and the same volume of water was added. EGCG stock solution were added dropwise and mixed for 1 h (molar ratio of EGCG/BLG was 4 : 1). The obtained samples were freeze-dried and put in a refrigerator for further use.

Particle diameter and zeta-potential analysis. The droplet size (Dz), polydispersity index (PDI), and zeta-potential of the samples was analyzed by Zetasizer Nano (Malvern Instruments, Worcestershire, UK).[37] All DLS measurements were performed in triplicate at 25 °C. The refractive index values used for the BLG nanoparticles and the aqueous phase were 1.45 and 1.33, respectively.

Loading amount and encapsulation efficiency. The loading amount and encapsulation efficiency of EGCG in BLG, and BLG–CA conjugate nanoparticles were analyzed with a recently reported method with minor modification.[29] Firstly, 2 mL of EGCG-loaded nanoparticles was transferred into an Amicon Ultra-3K centrifugal filter device (Millipore Corp., Billerica, MA, USA) with a low-binding Ultracel membrane (3000 MWCO). After centrifugation at 4000g for 30 min, free EGCG passed through the Ultracel membrane, while EGCG in complexes with BLG remained in the filter unit. The amount of EGCG in the ultrafiltrate was determined by HPLC described below.

The encapsulation efficiency (EE) and loading amount (LA) were calculated with the following equations:

$$EE \ (\%) = 100 \times \frac{total \ amount \ of \ EGCG - free \ EGCG \ in \ ultrafiltrate}{total \ amount \ of \ EGCG} \quad (3)$$

$$LA \ (mg \ g^{-1}) = \frac{loaded \ amount \ of \ EGCG}{total \ amount \ of \ nanoparticles} \quad (4)$$

Transmission electron microscopy (TEM) analysis. The shapes and characteristics of the EGCG loaded nanoparticles were visualized with TEM. All samples were prepared by the conventional negative-staining method. Nanoparticles redissolved in ultrapure water were placed on carbon-coated copper grids and then the samples were negatively stained with 2% (w/v) phosphotungstic acid (PTA). Grids bearing nano-particles were determined with a Hitachi H-700 transmission electron microscope (Hitachi, Tokyo, Japan).

Storage stability. Equal volumes (0.5 mL) of the EGCG and EGCG-loaded BLG nanoparticles or BLG–CA nanoparticles with the same concentration of EGCG were dispersed in 9.5 mL of pH 7.4 PB. At certain time intervals of 0, 0.5, 1, 2, 4, and 6 h, a 0.5 mL sample was withdrawn from each of the dispersion samples, and extracted with the same volume of ethyl acetate thrice. Fresh PB (pH 7.4, 0.5 mL) was replenished. After extraction, the ethyl acetate phase was rotary evaporated, redissolved in water, and analyzed using HPLC (as described below).

An Agilent 1100 HPLC system equipped with a DAD UV-vis absorption detector (Agilent, Santa Clara, CA) and a Nova-Pak C$_{18}$ 3.9 × 150 mm column (Waters) was used. The aqueous solution of 30% methanol containing 0.1% acetic acid was used as eluent with a flow-rate of 1.0 mL min^{-1} and the injection volume was 10 µL. The detection temperature was kept at 25 °C and the detection wavelength was 280 nm.[38]

***In vitro* release.** EGCG-loaded nanoparticles in the filter unit were collected and used for the determination of the *in vitro* release profile. The samples were dispersed in simulated gastric fluid (SGF) or simulated intestinal fluid (SIF), which was immediately placed in the dialysis bags (MWCO 3.5 kDa). The mass ratio between BLG and pepsin is 20 : 1 (w/w).[39] SGF was 0.1 M HCl (pH 1.5) containing 0.1% pepsin. SIF is mainly composed of 50 mM PB (pH 6.5) with 0.2% pancreatin and

0.25% bile salts. For gastric digestion, the dialysis bags containing SGF were put in acid release medium I (0.1 M HCl, pH 1.5). For intestinal stage, the dialysis bags containing SIF were put in release medium II (50 mM PB, pH 6.5). Aliquots of dissolution medium (0.5 mL) were withdrawn at certain time intervals, and the concentration of EGCG was determined by HPLC as described above. The same volume of buffer (0.5 mL) was fed back to the release media. The percent cumulative amount of EGCG released from the nanocomplexes was calculated as a function of time.

Statistics. All tests were measured in triplicate, and all data were expressed as mean ± standard deviation. The data were analyzed by the analysis of variance (ANOVA) using the SPSS 17.0 package (IBM, New York). Duncan's multiple-range test was used to determine the significant differences of mean values. Differences with $P < 0.05$ was considered statistically significant.

Results and discussion

CA conjugation optimization

The hydroxyl radicals, generated by the reaction between L-ascorbic acid and H_2O_2, can react with the side chain of sensitive amino residues (tryptophan, lysine, and cysteine) of a protein, producing radical species on its structure. The radical species react with phenolic acid producing protein–phenolic acid covalently grafted conjugates.[26] The more phenolic acid conjugated, the higher the antioxidant activity of the protein–phenolic acid conjugate. BLG–CA conjugates with various mass ratios of CA to BLG (0.1 : 1, 0.25 : 1, 0.5 : 1, 0.75 : 1, and 1 : 1) were prepared and the conjugation degree was estimated to obtain the optimal BLG–CA conjugates. As shown in Fig. 1, lowest amount of CA was bound to BLG (31.3 mg g^{-1}) at mass ratio of 0.1 : 1 (CA : BLG). The conjugation degree increased with the increase of the CA : BLG mass ratio between 0.1 : 1 to 0.5 : 1. Whereas, CA substitution reached a plateau when further increase the mass ratio. The conjugation amounts were

102.1, 106.8, and 107.7 mg g^{-1}, corresponding to the mass ratio of CA to BLG of 0.5 : 1, 0.75 : 1, and 1 : 1, respectively. No significant differences were observed for these three mass ratios. However, the efficiency decreased with the increase of mass ratio between CA and BLG. The substitution efficiency decreased from 32.4% to 12.1% with the increase of CA : BLG mass ratio from 0.1 : 1 to 1 : 1.

Characterization of BLG–CA conjugates

SDS-PAGE. SDS-PAGE is widely used to study and confirm the conjugation of reducing sugar and protein or protein and polyphenols.[27,28] SDS and As can be observed in Fig. 2, a clear band, corresponding to native BLG with molecular weight of 18.2 kDa, was observed in lane 2. A small amount of BLG dimer at 38.4 kDa was also detected.

The molecular weight of BLG increased after CA conjugation at CA : BLG of 0.1 : 1, indicating CA was successfully conjugated onto BLG with the free radical method. There is an increase in the molecular weight of BLG with the increase of the weight ratio of CA : BLG from 0.1 : 1 to 0.5 : 1, indicating more CA was covalently bound to BLG. Similar results were also reported by Rawel et al.[40] The increase of the molecular weight of BLG dimer was also found when the weight ratio of CA : BLG increased. This was consistent with the phenolic acid determination results. However, further increasing of mass ratio resulted in no appreciable increase of BLG's molecular weight. Similar results were also reported in grafting gallic acid onto chitosan.[41] It is likely that all available binding sites on BLG were saturated with CA at the CA : BLG mass ratio of 0.5 : 1.

It is important to note that little CA non-covalently bound to BLG through hydrophobic interactions and hydrogen bonding may exist,[21] possibly leading to the increase of bound CA and the increase of antioxidant activity of BLG–CA conjugate.
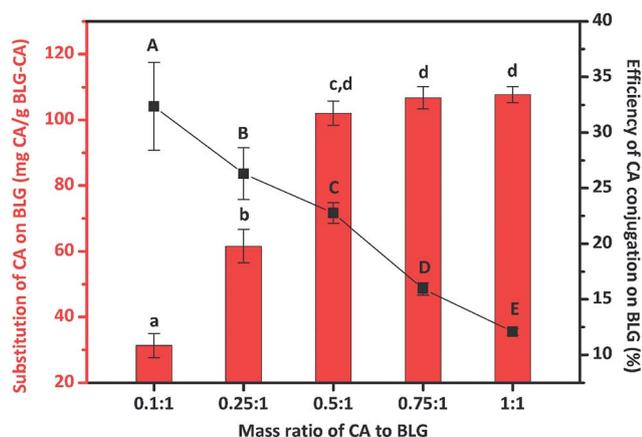

Fig. 1 Impact of the various mass ratios of chlorogenic acid (CA) to β-lactoglobulin (BLG) on the substitution and conjugation efficiency of CA on BLG. Values with different letters (a–d; A–E) are significantly different ($p \leq 0.05$).
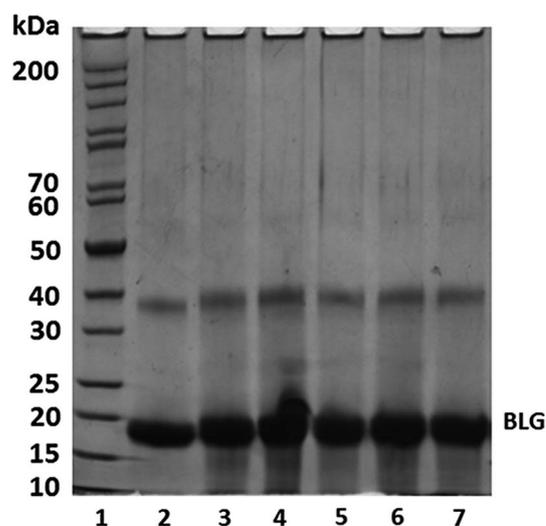

Fig. 2 SDS-PAGE results of BLG and BLG–CA conjugates under reducing conditions. Lanes: 1, protein markers; 2, BLG (control); 3–7, BLG–CA conjugates synthesized at different mass ratio of CA : BLG (0.1 : 1, 0.25 : 1, 0.50 : 1, 0.75 : 1, and 1 : 1, respectively).
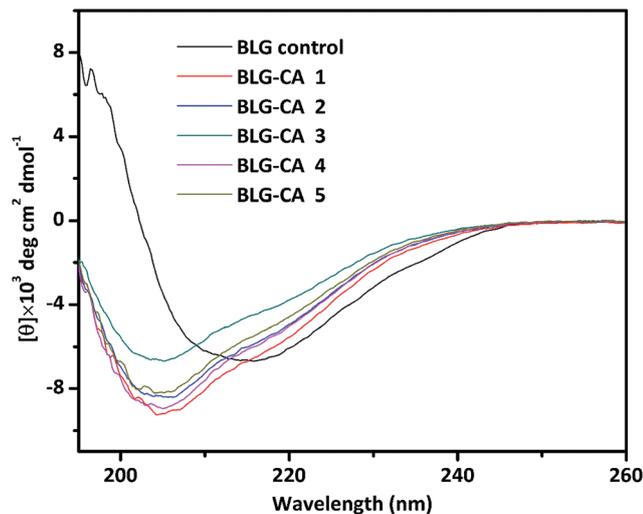
Fig. 3 Far-UV CD spectra (195–260 nm) of BLG control, and BLG–CA conjugates obtained at different mass ratio of CA : BLG (0.1 : 1, 0.25 : 1, 0.50 : 1, 0.75 : 1, and 1 : 1, respectively).

Far UV CD. The negative peak at 216 nm of far-UV CD spectrum indicates that BLG is rich in β-sheet secondary structure (Fig. 3). Based on the calculation from far-UV CD spectra data using DichroWeb online, the secondary structure of BLG (10 mM PB, pH 7.0, 20 °C) was found to be consisted of 18.1% α-helix, 38.3% β-sheet, 18.7% β-turn, and 25.2% random coil structure (Table 1). This is in agreement with previous literature findings.[23,28] After CA conjugation, the wavelength of negative peak at 216 nm was shifted to 206 nm, indicating changes occurred in BLG's secondary structure. The secondary structure compositions of five BLG–CA conjugates were calculated with DichroWeb online and shown in Table 1. CA conjugations led to the decrease of α-helix and β-sheet with the corresponding increase of β-turn and random coil. The results suggested that BLG unfolding occurred with CA conjugation. It is noteworthy that no significant differences were observed between five different BLG–CA conjugates with various conjugation degrees. Far UV CD results clearly demonstrated that CA was successfully covalently bound to BLG molecules.

Table 1 Secondary structure composition of BLG and BLG–CA conjugates prepared with various CA : BLG mass ratios (0.1 : 1 to 1 : 1) from far UV CD[a]

Samples	α-Helix (%)	β-Sheet (%)	Turns (%)	Unordered (%)
BLG	18.1	38.3	18.7	25.2
BLG–CA conjugate 1	11.9	27.8	20.6	37.6
BLG–CA conjugate 2	10.7	30.2	19.7	35.7
BLG–CA conjugate 3	7.6	24.8	21.9	41.7
BLG–CA conjugate 4	9.7	29.7	21.4	36.3
BLG–CA conjugate 5	11.2	30.2	19.2	38.4

[a] The secondary structure composition was calculated from far-UV CD spectra data using DichroWeb online (http://dichroweb.cryst.bbk.ac.uk/html/home.shtml).

ATR-FTIR. The ATR-FTIR spectra (4000–650 cm^{-1}) of native BLG, and BLG–CA conjugates prepared at five different mass ratio were shown in Fig. 4A. The spectrum and the curve-fitting components of the deconvolved amide I region (1700–1600 cm^{-1}) of BLG after CA conjugation was shown in Fig. 4B. Bands in this region correspond to α-helix, β-sheets, turns, and random coils.[34,42] The percentages of the secondary structures were summarized in Table 2. Native BLG has 12.0% α-helix, 57.3% β-sheet, 16.0% turns, and 14.7% unordered in our study, similar to previous reports.[43] It's worth noting that the percentage of secondary structure of BLG obtained with ATR-FTIR is significantly different with that obtained with far UV CD. Different testing mechanism and calculation may be one reason. Another reason was due to different water amount. Reports showed that dehydration could lead to the increase of β-sheet at the expense of α-helix.[44] Even though, both methods showed the similar changes of BLG after CA conjugation. ATR-
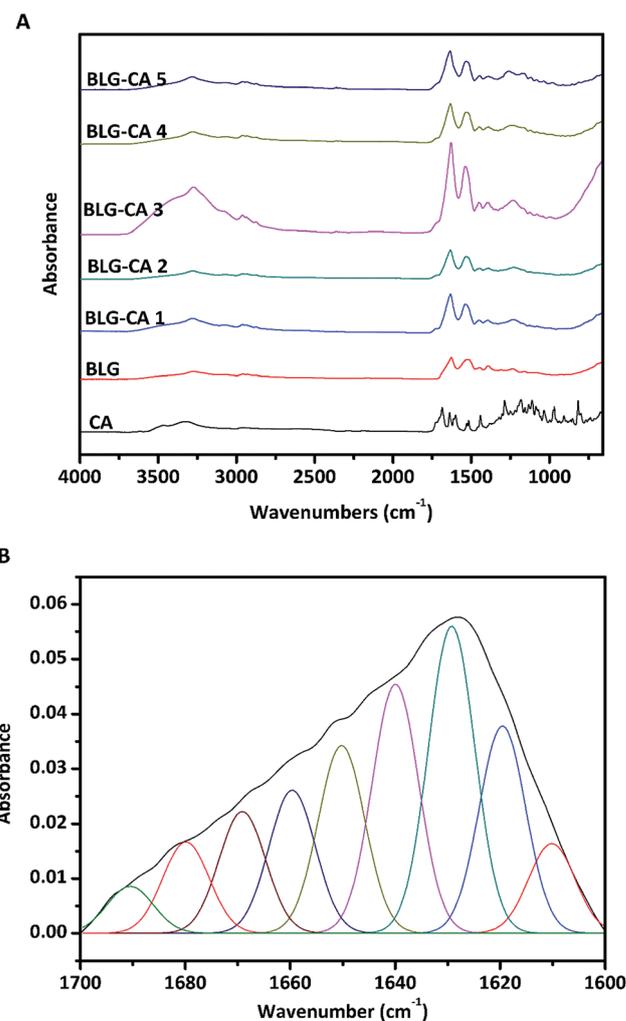

Fig. 4 ATR-FTIR spectra (A) of BLG control, and BLG–CA conjugates obtained at different mass ratio of CA : BLG (0.1 : 1, 0.25 : 1, 0.50 : 1, 0.75 : 1, and 1 : 1, respectively). Deconvolution of the spectra (B) depicted detailed secondary structure profiles in the amide I band region of BLG (1700–1600 cm^{-1}).

Table 2 Secondary structure composition of BLG and BLG–CA conjugates prepared with various CA : BLG mass ratios (0.1 : 1 to 1 : 1) from ATR-FTIR[a]

Samples	α-Helix (%)	β-Sheet (%)	Turns (%)	Unordered (%)
BLG	12.0	57.3	16.0	14.7
BLG–CA conjugate 1	9.1	49.3	23.4	18.1
BLG–CA conjugate 2	8.7	47.2	22.1	22.0
BLG–CA conjugate 3	8.4	47.3	26.3	18.0
BLG–CA conjugate 4	7.9	50.6	21.7	19.9
BLG–CA conjugate 5	8.3	46.1	23.0	22.5

[a] The secondary structure composition was calculated from ATR-FTIR curve-fitting individual components.

FTIR results displayed that the secondary structure of BLG changed toward to a higher turns and random coils at the expense of α-helix and β-sheet after CA conjugation, consistent with far UV CD results. No correlation between the CA conjugation amount and the extent of secondary structure changes was found. ATR-FTIR results also revealed that CA was successfully covalently bound to BLG molecules.

Antioxidant activity of BLG–CA conjugate

DPPH radical scavenging ability. To investigate the effects of various CA conjugation on the antioxidant activity of BLG–CA conjugate and the *in vitro* profile as well as chemical stability of EGCG in BLG, or BLG–CA conjugates nanoparticle, two BLG–CA conjugates low (31.3 mg g^{-1}) and high (102.1 mg g^{-1}) were used in the following study.

The DPPH radical scavenging abilities of BLG, BLG–CA (low), BLG–CA (high), and CA were shown in Fig. 5A. DPPH radical scavenging ability increased with the increase of concentrations for all samples (BLG, BLG–CA (low), BLG–CA (high), and CA). BLG was reported to have anti-oxidative activity mainly due to cysteine-121 group.[45] However, BLG showed the least DPPH radical scavenging ability in this study. The value was only 9.8% at the highest concentration (1 mg mL^{-1}). After CA conjugation, the DPPH radicals scavenging ability was significantly improved. At 0.1 mg mL^{-1}, the value was 22.3% and 30.3% for BLG–CA (low) and BLG–CA (high), respectively. BLG–CA (high) has better DPPH radical scavenging ability than BLG–CA (low). CA exhibited greatest ability in scavenging DPPH radicals for its strong hydrogen-donating ability. The value was 92.5%, which was remarkably higher than both BLG–CA conjugates at the same concentration. DPPH radical scavenging abilities increased with the increase of the concentration of both BLG–CA conjugates. At 0.6 mg mL^{-1}, the values were 91.8%, 92.6% and 93.0% for BLG–CA (low), BLG–CA (high) and CA, respectively. No significant differences were observed for either BLG–CA conjugates or CA when concentration is higher than 0.6 mg mL^{-1}.

Reducing power. Reducing power assay, which monitors the reduction of Fe^{3+} to Fe^{2+} by antioxidants, has been extensively used for antioxidant activity determination. As shown in Fig. 5B, the reducing power of all samples (BLG, BLG–CA (low), BLG–CA (high), and CA) increased with the increase of their
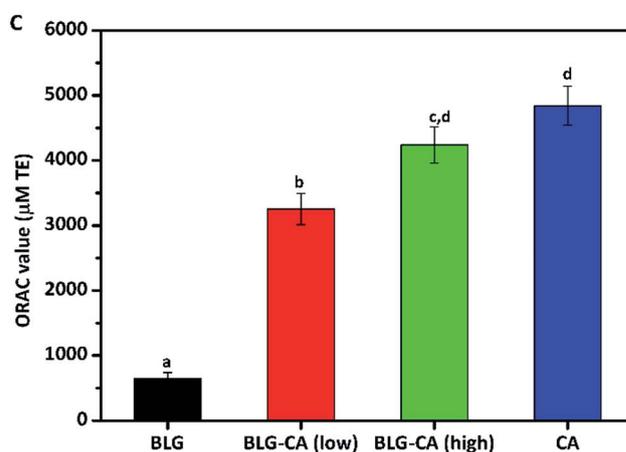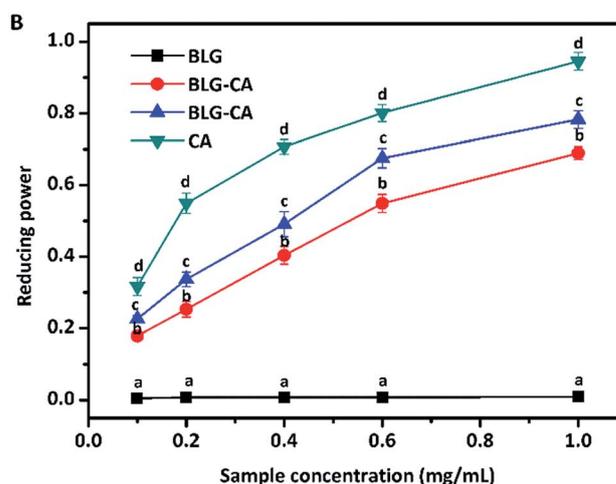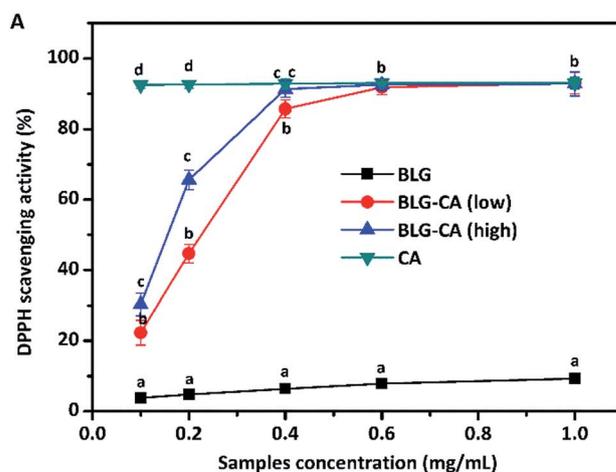

Fig. 5 Antioxidant activity (DPPH scavenging ability, oxygen-radical antioxidant capacity (ORAC), and reducing power) of BLG, BLG–CA conjugate, and CA. Values at the same concentration with different letters (a–d) are significantly different ($p \leq 0.05$).

concentration as expected. CA showed the highest reducing power at all concentrations among three samples for its strong hydrogen-donating ability. BLG–CA (high) exhibited higher

reducing power than BLG–CA (low) at all concentration (0.1–1.0 mg mL^{-1}). The reducing power of BLG–CA (low) conjugate was 0.689, while the value was 0.783 for BLG–CA (high) conjugate at 1.0 mg mL^{-1}. The reducing power of BLG (native) was negligible (only 0.009) (Fig. 5B). The results clearly indicated the reducing power of BLG were greatly enhanced after conjugation with CA.

Oxygen radical antioxidant capacity (ORAC). ORAC assay has also been widely used for antioxidant activity evaluation of functional bioactive compounds. As expected, BLG–CA showed remarkably higher oxygen radical scavenging ability than BLG (Fig. 5C). The ORAC values were 646.5, 3254.5, 4237.4, and 4840.4 for BLG, BLG–CA (low), BLG–CA (high), and CA, respectively. BLG–CA conjugates exhibited more than 5 times (5.0 and 6.6 for BLG–CA (low) and BLG–CA (high), respectively) higher ORAC value than BLG. BLG–CA (high) showed higher ORAC value than BLG–CA (low) for the higher CA conjugation degree.

The above results (DPPH radical scavenging ability, reducing power, and ORAC value) obviously suggested that BLG–CA conjugate can be used as an effective stabilizer for nutraceuticals protection, encapsulation, and delivery.

Characterization of EGCG-loaded BLG–CA conjugate nanoparticle. The characteristics (Z-average, zeta-potential, EE, and LA) of EGCG-loaded BLG nanoparticles were shown in Table 3. The particle diameters were 110.3, 107.4, and 105.8 nm with DLS (dynamic light scattering), respectively for EGCG-loaded BLG, BLG–CA conjugate (low), and BLG–CA conjugate (high) nanoparticles; and their zeta-potentials were −44.3, −45.6, and −47.7 mV, respectively ($P > 0.05$). The EE of EGCG in BLG, BLG–CA (low), and BLG–CA (high) nanoparticles were 72.9%, 71.8%, and 73.5%, respectively. The LA of EGCG loaded in BLG, BLG–CA (low), and BLG–CA (high) were 7.3%, 7.2%, and 7.4%, respectively. No significant differences were observed for EE and LA. Covalently bound CA may not have significant impacts on the interfacial properties and emulsifying ability of BLG, resulting in no particle size, zeta-potential, EE and LA changes of EGCG-loaded nanoparticles.

TEM results showed that both BLG–CA (low) and BLG–CA (high) nanoparticles were spherical, homogeneous, and uniform (Fig. 6). The mean particle sizes were less than 50 nm, far smaller than the results obtained with DLS. Similar results was also reported.[10] This is mainly attributed to that DLS data were obtained in solution where nanoparticles were fully hydrated, while TEM images were got in a dry state on carbon-coated copper grid.
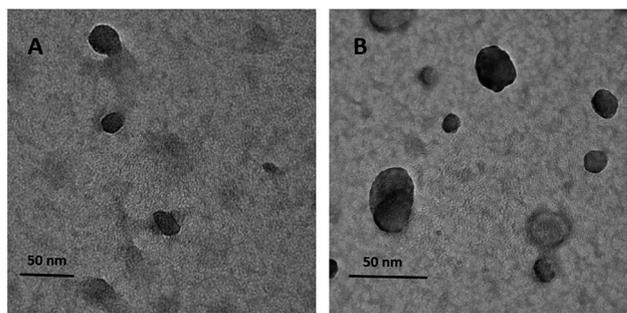

Fig. 6 Transmission electron microscopy (TEM) images of EGCG-loaded nanoparticles. EGCG encapsulated with BLG–CA (low) nanoparticles (A), and EGCG encapsulated with BLG–CA (high) nanoparticles (B). The mass ratio of CA to BLG was 1 : 2. The scale bar represents 50 nm in both (A) and (B).

Chemical stability of EGCG in nanoparticles. EGCG is very unstable at neutral and mild alkaline solution, which decrease the bioavailability and the potential health effects. As shown in Fig. 7, EGCG was rapidly degraded at pH 7.4 PB buffer during 6 h of storage. Almost half of EGCG lost after only 2 h. EGCG's
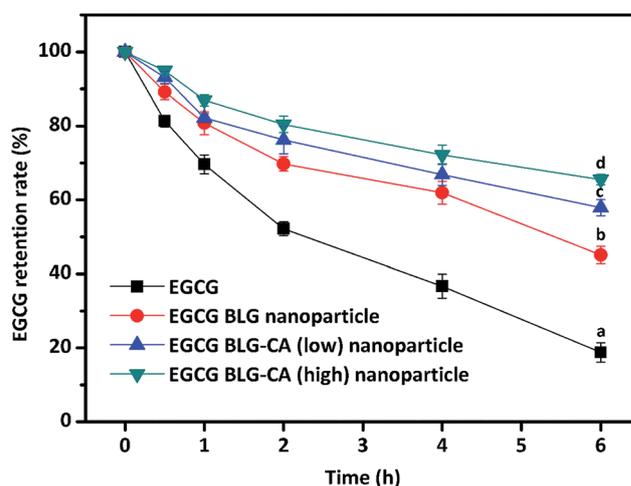

Fig. 7 Chemical stabilities of free EGCG and EGCG in nanoparticles during storage. The chemical stabilities of free EGCG (black square), EGCG-loaded BLG nanoparticles (red circle), BLG–CA (low) (blue triangle), and BLG–CA (high) nanoparticles (green inverse triangle) at pH 7.0 after 6 h at room temperature are shown. Values with different letters (a–d) at the same time intervals are significantly different ($p \leq 0.05$). Data are expressed as mean ± STD.

Table 3 Mean particle size, zeta-potential value, encapsulation efficiency (EE), and loading amount (LA) of EGCG in BLG, and BLG–chlorogenic acid conjugate nanoparticle[a]

Sample	Mean particle diameter (nm)	Zeta-potential (mV)	EE (%)	LA (%)
BLG	110.3 ± 3.2 (a)	−44.3 ± 1.6 (a)	72.9 ± 1.3% (a)	7.3 ± 0.1% (a)
BLG–CA conjugate (low)	107.4 ± 2.0 (a)	−45.6 ± 2.1 (a)	71.8 ± 1.4% (a)	7.2 ± 0.2% (a)
BLG–CA conjugate (high)	105.8 ± 1.7 (a)	−47.7 ± 2.3 (a)	73.5 ± 1.5% (a)	7.4 ± 0.2% (a)

[a] Significant differences within a column are denoted with letters (a) ($P < 0.05$).

chemical stability was significantly enhanced with nano-encapsulation. At 0.25 h, the retention rate of free EGCG was 81.4%. While the values were 89.2%, 93.1%, and 94.9%, in BLG, BLG–CA (low), and BLG–CA (high) nanoparticles, respectively. Only 18.8% of EGCG was left after 6 h incubation. Whereas, 45.1% 57.9%, and 65.5% of EGCG still remained for BLG, BLG–CA (low), and BLG–CA (high) nanoparticles respectively. It is noteworthy that both BLG–CA conjugates showed better protection for EGCG than BLG. Furthermore, the retention rate of EGCG in BLG–CA (high) nanoparticle was greatly higher than that in BLG–CA (low) nanoparticle. This was mainly attributed to the higher amount of covalently bound CA in BLG–CA (high). CA was an excellent antioxidant which can effectively reduce metal ion, scavenging free radicals and peroxyl radicals.

In vitro **release of EGCG nanoparticle in simulated gastrointestinal digestion.** EGCG can be released from nanoparticles under simulated gastrointestinal digestion mainly through diffusion and destruction of the nanoparticles structure by digestion.[46] Digestive enzymes may play a more important role. The *in vitro* release of EGCG from BLG, BLG–CA conjugate (low), and BLG–CA conjugate (high) nanoparticles in a simulated gastric environment is shown in Fig. 8A. Few EGCG was released in the

whole gastric stage during 3 h incubation. After 3 h, only 17.1%, 15.5%, and 14.2% of EGCG was released from BLG, BLG–CA conjugate (low), and BLG–CA conjugate (high) nanoparticles, respectively. The mean particle size did not show significant changes during whole gastric digestion (data not shown), suggesting BLG was resistant to proteolysis of pepsin. Similar results were also reported that BLG was resistant to pepsin-hydrolysis.[23,39] The extent of EGCG release from BLG–CA conjugate nanoparticles was relatively lower than that from BLG nanoparticles. The information obtained in this study was consistent with the results observed by Hu *et al.*,[29] who showed that the release of EGCG from chitosan nanoparticles under gastric condition can be controlled with phenolic acid grafting. It was also reported that the activity of digestive enzymes (such as amylase, protease and lipase) can be remarkably inhibited by polyphenols.[47,48] Conjugated CA retarded pepsin catalytic activity in this study.

At the intestinal stage, all three nanoparticles showed a rapid release of EGCG at the beginning and a sustained release of EGCG during the whole digestion process. After the first 30 min of digestion, 35.1, 28.6, 17.7% of EGCG were released in BLG, BLG–CA (low), and BLG–CA (high) nanoparticles, respectively. The release of EGCG was relatively slow from BLG–CA conjugates nanoparticle than from BLG nanoparticle ($p < 0.05$). After 4 h of digestion with pancreatin, the extents of EGCG release were 48.3%, 40.3%, 32.7% for BLG, BLG–CA conjugate (low), and BLG–CA conjugate (high) nanoparticles, respectively. The results indicated that covalently conjugated CA inhibited the activity of the digestive enzyme, which led to the reduction of the release rate and extent of EGCG. Furthermore, the release of EGCG was further inhibited with the increase of CA conjugation degree.

In conclusion, BLG–CA conjugate was prepared by the free radicals method and characterized with SDS-PAGE, far UV-CD, and ATR-FTIR. SDS-PAGE results clearly suggested that CA was successfully covalently bound to BLG. α-Helix and β-sheet structure of BLG decreased with a corresponding increase of turns and unordered structure after CA conjugation. The mean particle diameters of EGCG-loaded BLG or BLG–CA (low) and (high) nanoparticles were all approximately between 105 and 110 nm. BLG–CA showed better protection than BLG against EGCG degradation or oxidation. Simulated gastric digestion of EGCG-loaded nanoparticles showed limited release of EGCG, indicating they could potentially be used as vehicles for protection of EGCG in the stomach, and for its sustained release in the intestine. The release of EGCG from BLG–CA nanoparticles was slower and less than that from BLG nanoparticles. BLG–CA (high) showed higher inhibition of EGCG release than BLG–CA (low), suggesting that CA exhibited inhibition for digestive enzymes in intestinal stage. The results demonstrated the potential benefits of using BLG–CA conjugate as nanocarriers for nutraceuticals.
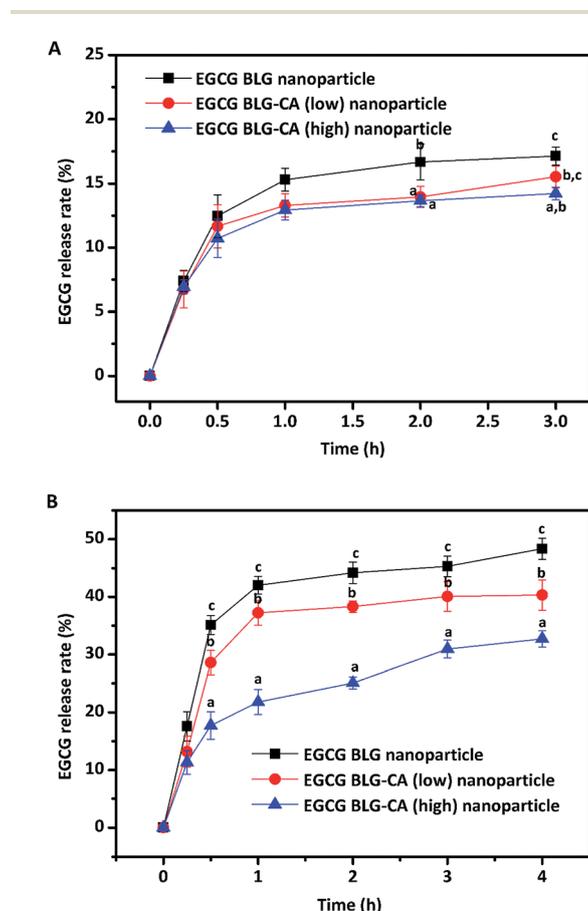

Fig. 8 *In vitro* release of EGCG in nanoparticles digested with pepsin and pancreatin at simulated gastrointestinal juice. Values with different letters (a–c) at the same time intervals are significantly different ($p \leq 0.05$). Data are expressed as mean ± STD.

Acknowledgements

References

1 N. Khan, F. Afaq, M. Saleem, N. Ahmad and H. Mukhtar, *Cancer Res.*, 2006, **66**, 2500–2505.

2 D. G. Nagle, D. Ferreira and Y.-D. Zhou, *Phytochemistry*, 2006, **67**, 1849–1855.

3 Y. He and F. Shahidi, *J. Agric. Food Chem.*, 1997, **45**, 4262–4266.

4 Y.-H. Kao, H.-H. Chang, M.-J. Lee and C.-L. Chen, *Mol. Nutr. Food Res.*, 2006, **50**, 188–210.

5 B. N. Singh, S. Shankar and R. K. Srivastava, *Biochem. Pharmacol.*, 2011, **82**, 1807–1821.

6 M. Nakao, S. Takio and K. Ono, *Phytochemistry*, 1998, **49**, 2379–2382.

7 Y. D. Jung, M. S. Kim, B. A. Shin, K. O. Chay, B. W. Ahn, W. Liu, C. D. Bucana, G. E. Gallick and L. M. Ellis, *Br. J. Cancer*, 2001, **84**, 844–850.

8 Y. Lun Su, L. K. Leung, Y. Huang and Z.-Y. Chen, *Food Chem.*, 2003, **83**, 189–195.

9 A. Dube, J. A. Nicolazzo and I. Larson, *Eur. J. Pharm. Sci.*, 2010, **41**, 219–225.

10 S. Kumar, R. Meena and P. Rajamani, *J. Agric. Food Chem.*, 2016, **64**, 6024–6034.

11 M. C. Bohin, J.-P. Vincken, H. T. W. M. van der Hijden and H. Gruppen, *J. Agric. Food Chem.*, 2012, **60**, 4136–4143.

12 P. Lestringant, A. Guri, İ. Gülseren, P. Relkin and M. Corredig, *J. Agric. Food Chem.*, 2014, **62**, 8357–8364.

13 J. Xue, C. Tan, X. Zhang, B. Feng and S. Xia, *J. Agric. Food Chem.*, 2014, **62**, 4677–4684.

14 H. Enomoto, C.-P. Li, K. Morizane, H. R. Ibrahim, Y. Sugimoto, S. Ohki, H. Ohtomo and T. Aoki, *J. Agric. Food Chem.*, 2007, **55**, 2392–2398.

15 L. Liang and M. Subirade, *J. Phys. Chem. B*, 2010, **114**, 6707–6712.

16 Z. Teng, R. Xu and Q. Wang, *RSC Adv.*, 2015, **5**, 35138–35154.

17 C. D. Kanakis, I. Hasni, P. Bourassa, P. A. Tarantilis, M. G. Polissiou and H.-A. Tajmir-Riahi, *Food Chem.*, 2011, **127**, 1046–1055.

18 B. Li, W. Du, J. Jin and Q. Du, *J. Agric. Food Chem.*, 2012, **60**, 3477–3484.

19 A. Shpigelman, Y. Cohen and Y. D. Livney, *Food Hydrocolloids*, 2012, **29**, 57–67.

20 A. Shpigelman, G. Israeli and Y. D. Livney, *Food Hydrocolloids*, 2010, **24**, 735–743.

21 C. Yin, L. Yang, H. Zhao and C.-P. Li, *Food Res. Int.*, 2014, **64**, 855–863.

22 C. P. Li, H. Enomoto, S. Ohki, H. Ohtomo and T. Aoki, *J. Dairy Sci.*, 2005, **88**, 4137–4145.

23 J. Yi, T. I. Lam, W. Yokoyama, L. W. Cheng and F. Zhong, *J. Agric. Food Chem.*, 2014, **62**, 8900–8907.

24 B. M. Dunn, in *Current Protocols in Protein Science*, John Wiley & Sons, Inc., 2001, ps2103s25.

25 L. Polgár, *Cellular and Molecular Life Sciences CMLS*, 2005, vol. 62, pp. 2161–2172.

26 U. G. Spizzirri, F. Iemma, F. Puoci, G. Cirillo, M. Curcio, O. I. Parisi and N. Picci, *Biomacromolecules*, 2009, **10**, 1923–1930.

27 J. Yi, Y. Fan, Y. Zhang and L. Zhao, *Food Chem.*, 2016, **205**, 73–80.

28 J. Yi, Y. Zhang, R. Liang, F. Zhong and J. Ma, *J. Agric. Food Chem.*, 2015, **63**, 297–303.

29 B. Hu, F. Ma, Y. Yang, M. Xie, C. Zhang, Y. Xu and X. Zeng, *J. Agric. Food Chem.*, 2016, **64**, 3422–3429.

30 J. Yi, T. I. Lam, W. Yokoyama, L. W. Cheng and F. Zhong, *Food Hydrocolloids*, 2015, **43**, 31–40.

31 N. Dyballa and S. Metzger, *J. Visualized Exp.*, 2009, **30**, e1431.

32 J. Yi, T. I. Lam, W. Yokoyama, L. W. Cheng and F. Zhong, *J. Agric. Food Chem.*, 2014, **62**, 8900–8907.

33 K. Brew, F. J. Castellino, T. C. Vanaman and R. L. Hill, *J. Biol. Chem.*, 1970, **245**, 4570–4582.

34 A. S. Eissa, C. Puhl, J. F. Kadla and S. A. Khan, *Biomacromolecules*, 2006, **7**, 1707–1713.

35 A. Zulueta, M. J. Esteve and A. Frígola, *Food Chem.*, 2009, **114**, 310–316.

36 S. Ko and S. Gunasekaran, *J. Microencapsulation*, 2006, **23**, 887–898.

37 J. Yi, T. I. Lam, W. Yokoyama, L. W. Cheng and F. Zhong, *J. Agric. Food Chem.*, 2014, **62**, 1096–1104.

38 M. Ding, H. Yang and S. Xiao, *J. Chromatogr. A*, 1999, **849**, 637–640.

39 J. Maldonado-Valderrama, A. P. Gunning, P. J. Wilde and V. J. Morris, *Soft Matter*, 2010, **6**, 4908–4915.

40 H. M. Rawel, S. Rohn, H.-P. Kruse and J. Kroll, *Food Chem.*, 2002, **78**, 443–455.

41 B. Hu, Y. Wang, M. Xie, G. Hu, F. Ma and X. Zeng, *J. Funct. Foods*, 2015, **15**, 593–603.

42 G. Panick, R. Malessa and R. Winter, *Biochemistry*, 1999, **38**, 6512–6519.

43 L. Bekale, P. Chanphai, S. Sanyakamdhorn, D. Agudelo and H. A. Tajmir-Riahi, *RSC Adv.*, 2014, **4**, 31084–31093.

44 H. R. Costantino, K. Griebenow, P. Mishra, R. Langer and A. M. Klibanov, *Biochim. Biophys. Acta, Protein Struct. Mol. Enzymol.*, 1995, **1253**, 69–74.

45 H. C. Liu, W. L. Chen and S. J. T. Mao, *J. Dairy Sci.*, 2007, **90**, 547–555.

46 Z. Li and L. Gu, *J. Agric. Food Chem.*, 2014, **62**, 1301–1309.

47 R. Gonçalves, N. Mateus and V. de Freitas, *J. Agric. Food Chem.*, 2010, **58**, 11924–11931.

48 Q. You, F. Chen, X. Wang, Y. Jiang and S. Lin, *LWT–Food Sci. Technol.*, 2012, **46**, 164–168.